ACS OMEGA

Open Access

http://pubs.acs.org/journal/acsodf

Article

Multi-Physics Simulation of Tar-Rich Coal In Situ Pyrolysis with a Multiregion Homogenization Treatment

Qianhao Ye, Mingjie Li, Jingyuan Hao, Zibo Huang, and Jinjia Wei*

Cite This: ACS Omega 2023, 8, 32565−32579

Read Online

ACCESS | Metrics & More | Article Recommendations

ABSTRACT: The macroscopic multi-physics simulation of tar-rich coal in situ pyrolysis (TCISP) is conducted, in the fractured porous zone, by coupling heat transfer, fluid flow, and chemical reaction. A novel TCISP pattern of gas injection between fractured zones is proposed by treating the fractured porous zone as a homogeneous porosity gradient descending region. In this case, nearly 11,500 kg of oil can be produced within 6 months from a 10*10*1 m^3 area. The influence of the fractured zone and porosity are investigated. The results indicated that gas injection between fractured zones is more conducive to rapid production, compared with the traditional case where the gas injection is in the center. The temperature field is more uniform, which is conducive to maintaining the same reaction conditions and producing appropriate products. Inlet velocity has a positive effect on the increase of heat transfer rate but has a negative effect on heat transfer uniformity. There is an optimal inlet temperature of 973 K for the fastest heating rate. With the increase in temperature, the heat transfer uniformity gets worse. Increasing the height of the fractured zone is beneficial for the heating rate and heat transfer uniformity.

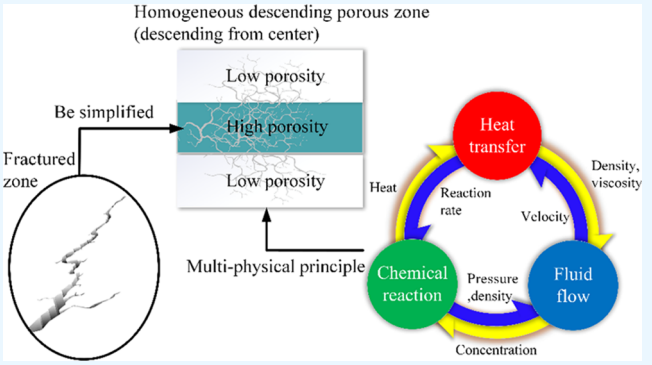

1. INTRODUCTION

Tar-rich coal is a kind of coal that contains about 8−12% tar (oil). Through pyrolysis, tar-rich coal can be transformed into energy and chemical raw materials such as tar and coal gas, which is significant for enhancing the utilization value of coal resources. However, the conventional ground pyrolysis process is accompanied by the discharge of wastewater and gas, resulting in a negative impact on the environment. In addition, underground coal gasification (UCG) will produce a large cavity underground and can easily cause stratum collapse. Tar-rich coal in situ pyrolysis (TCISP) refers to the technology that upgrades oil and gas products by heat transfer through heat carriers (such as high-temperature nitrogen) under formation pressure without mining, as shown in Figure 1. The products are expelled through pores and fractures in the coal layer and finally flow out through the production well on the right side. Compared with conventional pyrolysis, TCISP is a new and significant research field, which has a smaller footprint and a lower mining cost. It is a promising, economical, sustainable, and environmentally friendly technology.

As a new research field, there are few works of literature focused on TCISP. Similar fields mainly concentrate on underground pyrolysis of oil shale and underground coal gasification (UCG).

As for the underground pyrolysis of oil shale, the underground oil shale pyrolysis process by electric heating was studied first. Underground pyrolysis of oil shale is also known as in situ upgrading (ISU). Fan et al.[1] conducted the reservoir simulation through Stanford's GPRS framework. It is revealed that heating temperature is the major factor influencing gas production. Some scholars also focused on the ISU process with fluid injection. Maes et al.[2] studied the ISU through dimensionless analysis and optimized the heater temperature with the highest energy efficiency. Bauman et al.[3] used STARS CMG to simulate the field production process of ISU. The results showed that ISU can achieve a net energy benefit of 3:1, and an estimated carbon footprint of 36 kg CO_2/bbl oil production. Hao et al.[4] found that the oil production of underground oil shale pyrolysis with liquid injection is much greater than that without liquid injection. Its exploitation period is short and economic benefit is improved. Lei et al.[5] indicated a steam injection method to improve the

Received: May 6, 2023
Accepted: August 9, 2023
Published: August 31, 2023

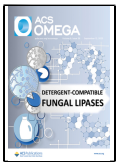

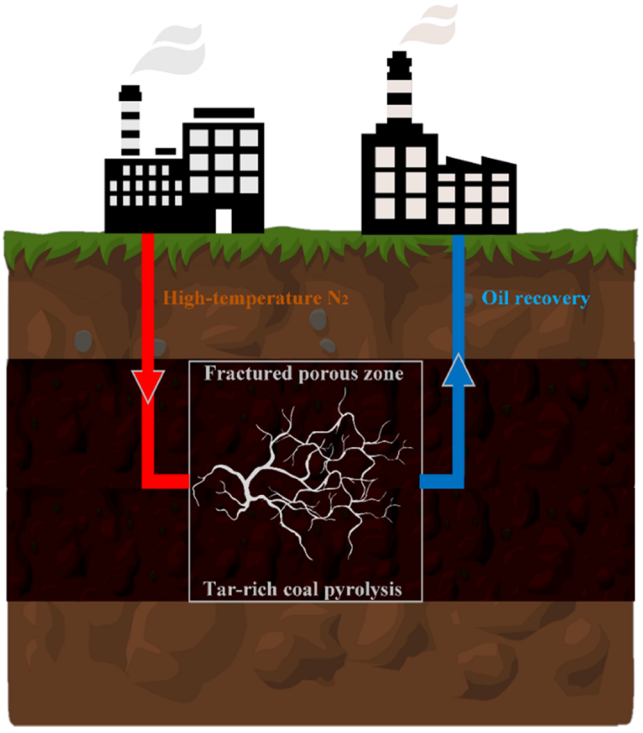

Figure 1. Schematic diagram of tar-rich coal in situ pyrolysis.

heat transfer rate in ISU, and the reservoir simulation results indicated that the temperature of oil shale in the process of steam injection is higher than that of electric heating. Pei et al.[6−9] conducted a series of studies on the gas-injected ISU process. The chemical reaction models were established based on the small-batch reactor results. The results suggest that air injection contributes up to 60% of the total heat transfer, and the square well pattern is the best. Varfolomeev et al.[10−12] pointed out that in the ISU process, crude oil undergoes three stages of transition at a constant inlet rate, namely, low-temperature oxidation (LTO), fuel deposition (FD), and high-temperature oxidation (HTO). Chen et al.[13,14] suggested that the oxidation reaction of oil can release a large amount of heat to raise the temperature of rocks and reservoir fluids, through air injection. The thermal effect of oxidation reaction has a significant contribution to oil recovery. Some researchers also pay attention to the evolution of pore structure by the combination of CT technology and three-dimensional (3D) reconstruction,[15−19] and these results are important for the further accurate study of pyrolysis characteristics.

The main differences between UCG and ISU are that the strata have different physical properties, and the reactions are different. In the study of UCG, the research mainly focuses on numerical simulation. Many different numerical models simulate the process of UCG. Yang and Liu[20] developed a two-dimensional free passage model of UCG to explore the change rules of the temperature field, concentration field, and pressure field in the coal seam. The packed bed reactor model was used by Yang et al.[21,22] A large-scale three-dimensional UCG simulation with a porous region was conducted by Seifi et al.[23,24] employing the STARS CMG. Based on the research, the results of the UCG process are more accurate compared with Yang et al.[21,22] because of the porous model. Nourozieh et al.[25] established a three-dimensional CFD model to simulate the large-scale linear controlled rollback injection point (L-CRIP) UCG process and calculated the syngas composition and final cavity. The effect of steam flux on the variation of syngas in UCG was investigated by Zogała and Janoszek[26] using a 3D numerical model. Wachowicz et al.[27]

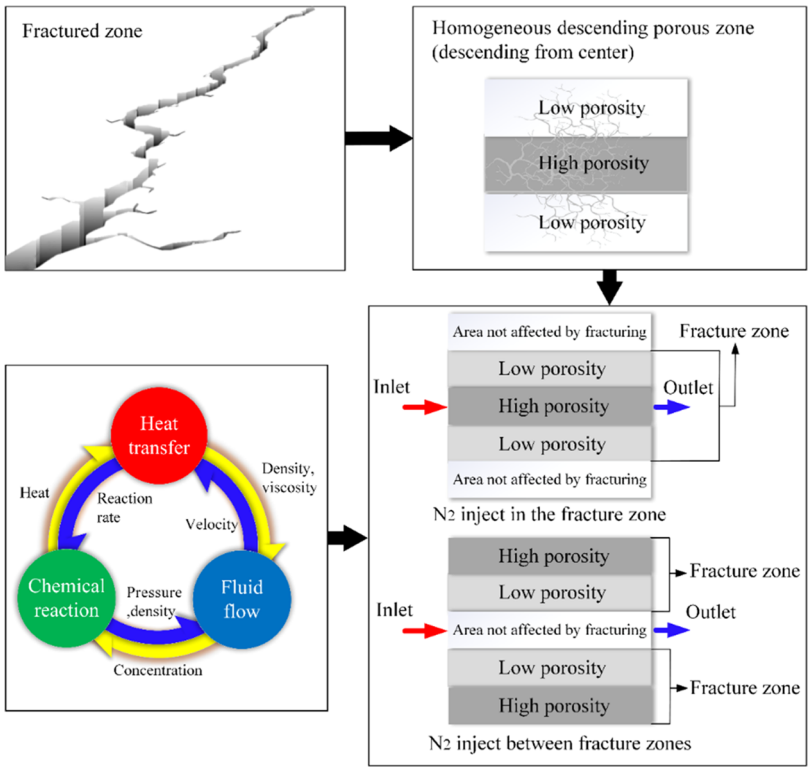

Figure 2. Fracture zone treatment and multiphysical principle analysis for TCISP.

https://doi.org/10.1021/acsomega.3c01481
ACS Omega 2023, 8, 32565−32579

and Gür and Canbaz[28] simulated the composition and temperature variation characteristics of syngas in the UCG process and verified them through experiments. In addition, the influence of coal seam structure change and cavity development on reaction and heat and mass transfer is studied comprehensively and in detail.[29,30] Based on the two-dimensional model, Gao et al.[31] simulated the growth of the cavity in the solid−gas conversion process through the porosity change model in UCG, and the simulation results were in good agreement with the experimental results.

In addition, TCISP is a typical problem of multi-physics and multiregion coupling in porous media. Research focusing on multi-physics simulation in porous media is helpful to solve this problem. Schaube et al.[32,33] investigated the performance of the CaO-$Ca(OH)_2$ reactor for thermochemical heat storage. Darcy's law is applied during the simulation. It was found that the thermal conductivity of the solid phase affects the reaction by affecting the heat transfer. Increasing thermal conductivity can increase the reaction rate. Shi et al.[34] focused on the same topic, used a similar method, and got similar results to Schaube et al.[32,33] Zhang et al.[35] used the digital twin model to simulate the flow and transport behavior of unconventional reservoirs. Combined with multiscale algorithms, the flow and transport phenomena are simulated. Zhang et al.[36] calculated the hydrogen phase equilibrium by coupling multi-physics and multiregion in porous media.

As a result of drilling, mining, and original cracks, underground coal seams form a large number of cracks. However, there are few macroscopic TCISP studies on the coupling of multiple physical fields in the fractured porous zone. Moreover, it is also a problem how to properly deal with the fractured porous media area under the comprehensive consideration of calculation accuracy and efficiency so that it can be used in engineering practice.

In this paper, the coupling of multiple physical fields in fractured porous media at a macro scale is studied utilizing numerical simulation due to the high cost, high risk, harsh experimental conditions, and difficulty in obtaining underground data. The research is conducted by Fluent with UDF attached. The simulation model is introduced and verified in Section 2. The influence of the structure of the porous crack zone, inlet velocity, inlet temperature, and height of the porous zone on heat transfer is studied and analyzed in Section 3. Furthermore, the production performance of TCISP was evaluated by the defined parameters of heating rate, heat transfer uniformity, and reaction area. Then, the conclusions are illustrated in Section 4.

2. MATHEMATIC MODELING AND NUMERICAL SIMULATION

2.1. Description of the Physical Problem and Geometric Model. A large-scale simulation considering the actual production practice is carried out. As a result of drilling, mining, and original cracks, underground coal seams form a fractured porous zone. A novel fractured porous zone treatment method that divided the calculation region into multi-homogeneous regions and multiphysical principle analysis for TCISP are illustrated in Figure 2. After drilling and fracturing the underground coal seam, there are many pores and fractures in the center of the coal seam, which gradually decrease in the surrounding areas. The coal seam is regarded as a homogeneous porous medium region, and the porosity gradient decreases from the center of the fracture zone to the surrounding area to simulate the distribution of the actual fractured zone (Figure 2 only shows the case fractured zone divided into three pieces, which can be adjusted according to the actual situation). The two cases in Figure 2 represent the two relative positions of the fractured zone and inlet in actual operation, respectively.

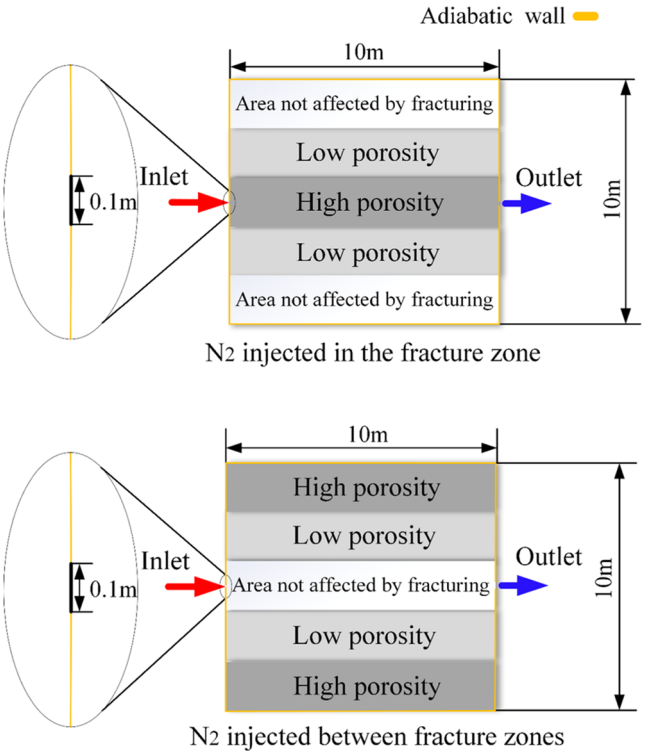

Figure 3. Geometric model and boundary conditions for the TCISP area.

As shown in Figure 2, the process of TCISP is a completely coupled multiphysical problem. The flow of gas affects the convective heat and mass transfer of components. The temperature affects the properties of the fluid and the flow of gas in the pores and cracks of the coal seam. The change of concentration mainly depends on the chemical reaction rate, and the chemical reaction process further depends on the temperature distribution. The chemical reaction process with heat releases or absorption in turn changes the temperature field of the coal seam. The rate of the chemical reaction is also affected by the concentration of reactants, which is affected by the gas diffusion and flow convection in the coal seam.

To reduce the computational cost of simulation and balance the computational efficiency and accuracy, the model adopts the following reasonable assumptions.

(1) The actual three-dimensional calculation is simplified into a two-dimensional calculation region to improve the calculation efficiency.
(2) Considering that the main heat transfer modes of coal seam underground are convection and conduction, radiation heat transfer is not considered in the TCISP process.
(3) There are a large number of cracks and pores in the fractured porous region, which could be simplified into a homogeneous porous medium region. In this region, the porosity descends from the center.

https://doi.org/10.1021/acsomega.3c01481
ACS Omega 2023, 8, 32565−32579

Table 1. Values and Formulas of the Main Parameters

parameter	values and formulas	unit
K	4.0×10^{-13}	m^2
λ_s	$\lambda_s = \lambda_{s0} - (\lambda_{s0} - 2.01)[\exp((T - 293.15)/(T + 403.15)) - 1]$	$W{\cdot}m^{-1}\ K^{-1}$
$c_{P,s}$	$c_{P,s} = c_{P,s0}(1 + \alpha T)$	$J{\cdot}kg^{-1}\ K^{-1}$
α	0.003	K^{-1}
λ_{s0}	0.3	$W{\cdot}m^{-1}\ K^{-1}$
$c_{P,s0}$	1300	$J{\cdot}kg^{-1}\ K^{-1}$
ΔH	201.30×10^3	$J{\cdot}mol^{-1}\ kg^{-1}$
A	10^9	s^{-1}
m	0.1	1
E_0	101.5×10^3	$J{\cdot}mol^{-1}$
R	8.314	$J{\cdot}mol^{-1}\ K^{-1}$

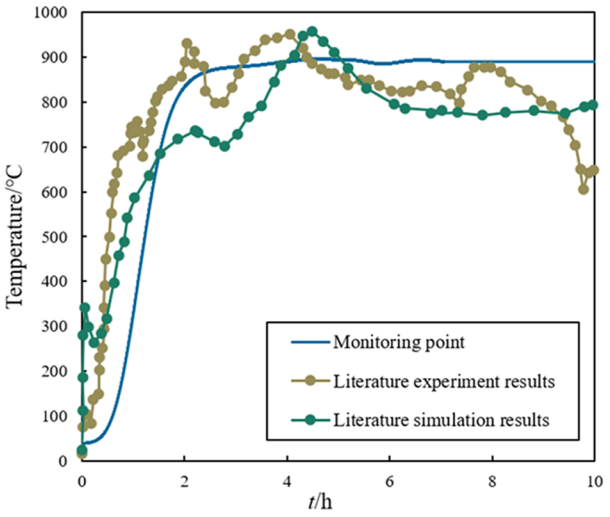

(a) The comparison of the temperature of the monitoring point

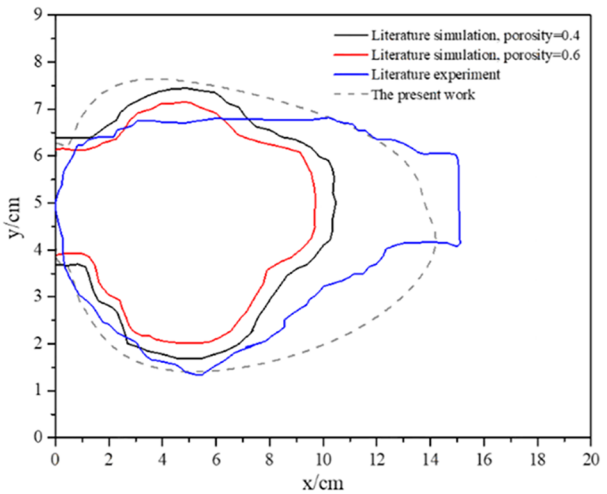

(b) The comparison of the cavity region and porosity

Figure 4. Comparison of the simulation results with the research of UCG.[31] Copyright 2021 Elsevier.

(4) The temperature of the pyrolysis reaction is generally higher than 537 K, under which the liquid tar would be gasified, so the reaction products are only gaseous and solid substances.

(5) During the reaction, the changes in stress and strain of the coal seam, porosity, and permeability of the solid are ignored.

The dimensions and boundary conditions of the geometric model are shown in Figure 3. The length of the calculation area is 10 m and the width is 10 m, which is determined by the drilling spacing and the measured width of the central coal seam. There is an entrance with a diameter of 0.1 m on the left, from which high-temperature nitrogen enters the calculation area, illustrated in Figure 3. Nitrogen provides heat as a heat carrier but does not react with the coal seam to ensure safety. The fluid flows out from the outlet with a diameter of 0.1 m on the right side. The vertical height of the exit and entrance is the same. The surrounding walls are adiabatic boundaries, painted in orange in Figure 3. Different porosity values are set for different areas of the coal seam in subsequent simulations.

2.2. Governing Equations. *2.2.1. Conservation Equations.* The gas energy equation is as follows:

$$(\varepsilon\rho_{g,i}c_{p_{g,i}})\frac{\partial T_{g,i}}{\partial t} + (\rho_{g,i}c_{p_{g,i}}\vec{v})\cdot\nabla T_{g,i} = \left(\varepsilon\frac{\partial P}{\partial t} + \vec{v}\cdot P\right) - \nabla\cdot(-\varepsilon\lambda_{g,i}\nabla T_{g,i}) \quad (1)$$

Solid energy equation:

$$((1\text{-}\varepsilon)\rho_s c_{ps})\frac{\partial T_s}{\partial t} = (1\text{-}\varepsilon)q_R\cdot\Delta H\text{-}\nabla\cdot(\text{-}(1\text{-}\varepsilon)\lambda_s\nabla T_s) \quad (2)$$

Gas continuity equation:

$$\frac{\partial((1\text{-}\varepsilon)\rho_s)}{\partial t} = (1\text{-}\varepsilon)q_R \quad (3)$$

Solid continuity equation:

$$\frac{\partial(\varepsilon\rho_{g,i})}{\partial t} + \nabla\cdot(\rho_{g,i}\vec{v}) = \text{-}(1\text{-}\varepsilon)q_R \quad (4)$$

where ε is the porosity, q_R is the mass reaction rate, which is given by the experimental reaction data, and subscript i represents the ith component gas.

$$q_R = (\rho_{coal}\text{-}\rho_{coal}')\frac{\partial X}{\partial t} \quad (5)$$

https://doi.org/10.1021/acsomega.3c01481
ACS Omega 2023, 8, 32565−32579

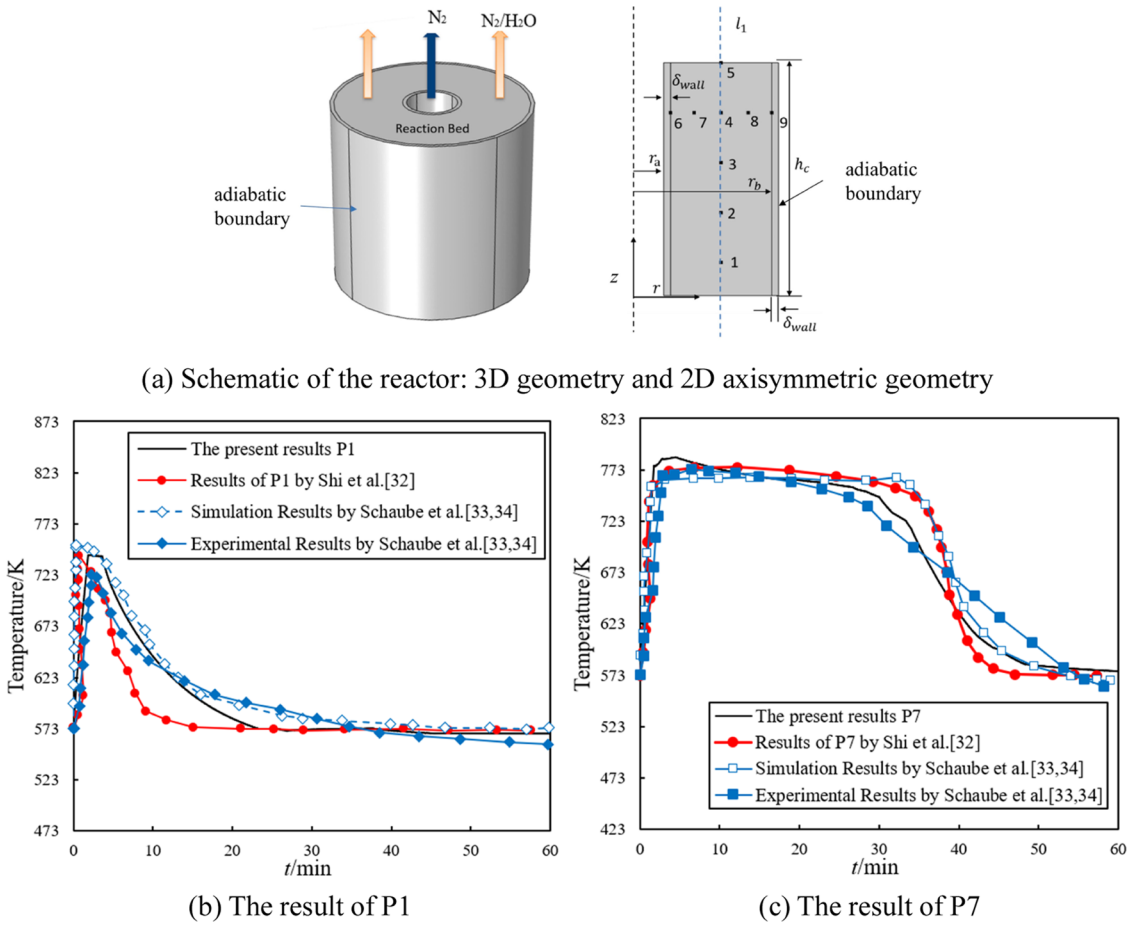

(a) Schematic of the reactor: 3D geometry and 2D axisymmetric geometry

(b) The result of P1

(c) The result of P7

Figure 5. Comparison of the simulation results with the research of thermochemical heat storage.[32−34] Copyright 2021, 2013 Elsevier.

Figure 6. Positions of the three sampling points.

where ρ_{coal} is the density of coal, ρ_{coal}' is the mass of the solid left after the pyrolysis reaction, and $\frac{\partial X}{\partial t}$ represents the reaction rate.

As for the momentum equation, the gas flow in the coal seam follows Darcy's law, which is known as:

$$\nabla P = -\frac{\mu_{g,i}}{K}\vec{v} \tag{6}$$

where ∇P is the pressure drop, $\mu_{g,i}$ is the viscosity of the gas, and K is the permeability whose value is 4.0×10^{-13} m^2.

The fluid viscosity, density, specific heat capacity, and thermal conductivity are calculated by eqs 7−9.

$$\mu_{gm} = \sum_{i=1}^{N} X_i \mu_{g,i} \cdots\cdots \left(\sum_{i=1}^{N} X_i = 1 \right) \tag{7}$$

$$\rho_{gm} = \sum_{i=1}^{N} X_i \rho_{g,i} \cdots\cdots \left(\sum_{i=1}^{N} X_i = 1 \right) \tag{8}$$

$$\lambda_{gm} = \sum_{i=1}^{N} X_i \lambda_{g,i} \cdots\cdots \left(\sum_{i=1}^{N} X_i = 1 \right) \tag{9}$$

The thermal conductivity and specific heat capacity of the solid could be obtained by eqs 10 and 11.

$$\lambda_s = \lambda_{s0} - (\lambda_{s0} - 1.96)\left[\exp\left(\frac{T - 293.15}{T + 403.15}\right) - 1\right] \tag{10}$$

$$c_{P,s} = c_{P,s0}(1 + \alpha T) \tag{11}$$

where α is 0.003 K^{-1}, λ_{s0} is 0.3 W·m^{-1} K^{-1}, and $c_{P,s0}$ is 1300 J·kg^{-1} K^{-1}.

2.2.2. Reaction Model. At present, the reaction data are obtained and estimated from in-house experimental data, as shown in eq 12.

https://doi.org/10.1021/acsomega.3c01481
ACS Omega 2023, 8, 32565−32579

$$\text{coal} \xrightarrow{673\ \text{K}} 0.172CH_4 + 0.135\text{tar} + 0.267C + 0.5\ \text{other solids} + 0.64CO_2 + 0.226CO + 0.6H_2O \quad (12)$$

where the heat of reaction ΔH = 201.30 kJ·mol^{-1} kg^{-1}. A modified Arrhenius equation is used to determine the reaction rate.

$$k = \frac{\partial X}{\partial t} = k_f A T^m e^{-E_0/RT} \quad (13)$$

where k_f is the correction coefficient, as shown in eq 14.

$$k_f = \begin{cases} 3.88 - 0.0033T & 773\ \text{K} < T < 873\ \text{K} \\ 0.0032T - 1.22 & 673\ \text{K} < T < 773\ \text{K} \end{cases} \quad (14)$$

The values and formulas of the main parameters measured by experiment and literature are listed in Table 1.

2.2.3. Model Verification. The numerical simulation results are first compared with the research of UCG,[31] based on the same reaction and conditions to verify the numerical model. As shown in Figure 4, with the increase of time, the variation of the simulation results is similar to the trend of the literature,[31] and the temperature difference in the process is small. Compared with the literature, the location and the final combustion cavity are consistent.

Then, to further validate the results, the simulation results are compared with the research on thermochemical heat storage[32−34] under the same conditions. The coordinates of P1 and P7 are (25, 10 mm) and (17, 55 mm), respectively. As shown in Figure 5, with the increase of time, the trend and the value of the simulation results are nearly consistent with the literature results. The temperature of monitoring points P1 and P7 illustrates the accuracy of the present study.

2.3. Definitions of Evaluation Index. To realize an excellent pyrolysis effect and enhance heat and mass transfer, the following parameters need to be defined to evaluate and analyze the pyrolysis process.

2.3.1. Heat Transfer Uniformity. The formula of heat transfer uniformity C was proposed to explain the uniformity in this problem, which is beneficial to maintaining the same reaction conditions and producing appropriate products. Subsequently, different working conditions were designed by changing the porosity, the size of the central region, and the flow rate at the entrance to explore the working condition that maximizes the heat transfer uniformity and achieves the best pyrolysis effect.

$$C = \frac{1}{(T_{in} - \bar{T})^2 + (T_{out} - \bar{T})^2 + \sum_{i=1}^{N} (T_{Ci} - \bar{T})^2} \quad (15)$$

where T_{in} is the inlet temperature, T_{out} is the outlet temperature, and T_{C1}, T_{C2}, ⋯, T_{CN} are the temperatures of the sampling points. In this paper, the value of N is 3, and the positions of the three points are shown in Figure 6, which represents the temperature of the center and the temperature near the edge. Heat transfer uniformity is calculated when the time instant is 3 months. When t is 3 months, the flow and heat transfer in the porous medium region under most working conditions are fully developed, the development of the high-temperature region is fast, and the heat and mass transfer are intense. The comparative analysis can better reflect the difference between different working conditions and compare the heat transfer uniformity.

2.3.2. Heating Rate. Set the heating rate as β to evaluate the heating time

$$\beta = \frac{1}{t} \quad (16)$$

where t is the heating time when the area average temperature is higher than 673 K (a significant pyrolysis reaction occurs between 673 and 873 K). The higher the heating efficiency β is, the better the heating effect is.

2.3.3. Reaction Region. Based on the experimental data, a significant pyrolysis reaction occurs between 673 and 873 K, so the region with a temperature above 873 K is regarded as the reaction region. The dimensionless parameter reacted region is defined as the ratio of the region area with a temperature higher than 873 K to the total region area.

$$R_f = \frac{S_f}{S} \quad (17)$$

2.3.4. Main Reaction Time. The elapsed time during which a significant pyrolysis reaction occurs within the temperature of 673−873 K is set as the main reaction time to describe and evaluate the extent to which the reaction proceeds.

3. RESULTS AND DISCUSSION

To explore and analyze the TCISP process, the influence of the fractured porous area, porosity, inlet temperature, inlet velocity, and height of the fractured porous region were investigated on heat transfer, mass transfer, and oil production under different working conditions.

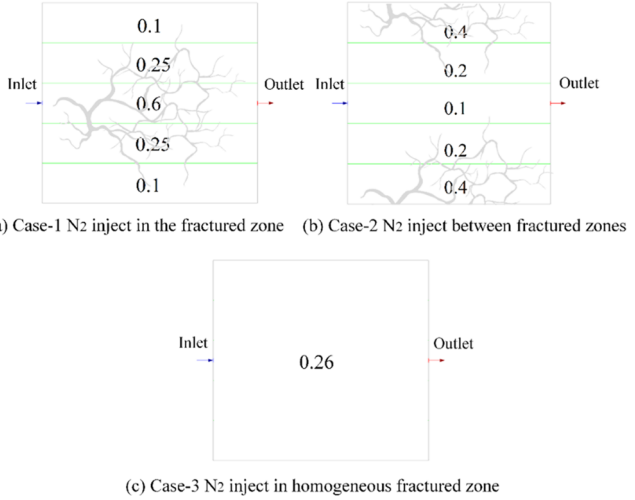

(a) Case-1 N2 inject in the fractured zone (b) Case-2 N2 inject between fractured zones

(c) Case-3 N2 inject in homogeneous fractured zone

Figure 7. Different fractured zones (Cases 1−3).

3.1. Effect of the Gas Injection Method. Mining or taking measures to fracture coal seams for heat and mass transfer enhancement will form some fractured zones. The effect of fractured zone porosity is investigated by the three practical cases in Figure 7. The numbers inside the region represent the porosity of the corresponding area. In Case 1 and Case 2, there exist fractured porous zones and in Case 3, the region is uniform in porosity. These cases share the same area average porosity for comparison.

As shown in Figures 8−10, the temperature field varies at different times. As time goes by, the inlet high-temperature nitrogen gradually diffuses in the fractured porous media area,

https://doi.org/10.1021/acsomega.3c01481
ACS Omega 2023, 8, 32565−32579

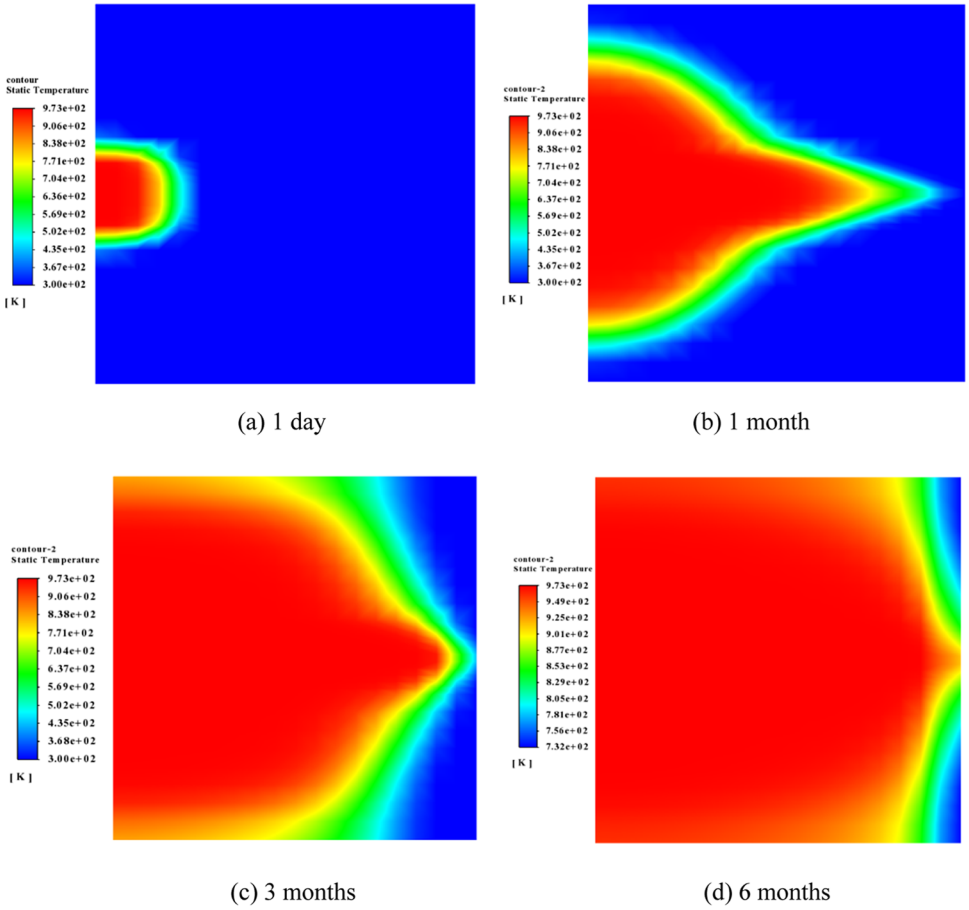

Figure 8. Temperature contours of N_2 injection in the center of the fractured zone (Case 1).

and the coal pyrolysis reaction takes place. Heat and mass transfer in multiple physical fields develops with time.

Especially, when the gas injection time is short (corresponding to Figures 8a,b, 9a,b, and 10a,b), the temperature field in Case 1 develops the fastest, followed by Case 3 and Case 2. This is because of the high porosity in the center of Case 1, the gas is easy to enter the region at the beginning and diffuses from the center to the periphery. Moreover, the contours in Case 1 are sharper compared to those in Case 2 and Case 3. The porosity in the center of Case 3 is 0.26, higher than 0.1 of Case 2, so the gas diffuses faster than in Case 2 in the beginning.

When the gas injection time is long (corresponding to Figures 8c,d, 9c,d, and 10c,d), on the contrary, the area of the high-temperature region in Case 2 is larger and the temperature distribution is more uniform, which is also suggested in Figure 11. In this case, the porosity in the periphery is larger, which is beneficial to the diffusion of gas around. Compared with Case 3, the temperature development of Case 1 is faster over time. The temperature development of Case 2 is faster at the later stage, and the temperature distribution of Case 2 is more uniform. Therefore, a fractured porous zone is recommended in practice.

To further investigate the influence of the fractured porous zone, Case 1 and Case 2 (where the fractured porous zone exists) are compared more carefully. As illustrated in Figure 11a,b, because the gas is easy to enter the region at the beginning, the temperature of Case 1 rises faster in the beginning. After that, the process that gas diffuses from the center to the periphery is dominant. With a larger periphery porosity, the temperature of Case 2 rises faster, the reaction region becomes larger. In the long production process, Case 2 is more conducive to the production of products and complete reaction.

Figure 12 suggests the final stable pressure drop of the three cases. It is illustrated that the homogeneous region (Case 3) is beneficial for decreasing the pressure drop. The more uneven the flow area, the greater the flow resistance.

Figure 13a suggests that Case 2 has the best heat transfer uniformity, Case 3 is worse than Case 2, and Case 1 is the worst. The N_2 injection between cracks (with increasing porosity gradient toward the boundary) is conducive to gas and heat diffusion to the boundary. As illustrated in Figure 13b, the oil production time in Case 2 is the most concentrated, followed by Case 1, and the oil production time in Case 3 is more evenly distributed over time. Therefore, Case 2 has the fastest rate of oil production, which is slightly lower than the other two cases. If a high yield is required in the short term, Case 2 is the best choice.

According to the analysis above, in the long production process, generating a fractured zone at the edge of the coal seam is more beneficial to the rapid production of products. In the process of gas injection, the temperature field of N_2 injection between cracks is more uniform, which is beneficial to maintain the same reaction conditions and produce appropriate products. In the following study, we took Case 2 (N_2 injection between cracks) as the benchmark to conduct

https://doi.org/10.1021/acsomega.3c01481
ACS Omega 2023, 8, 32565−32579

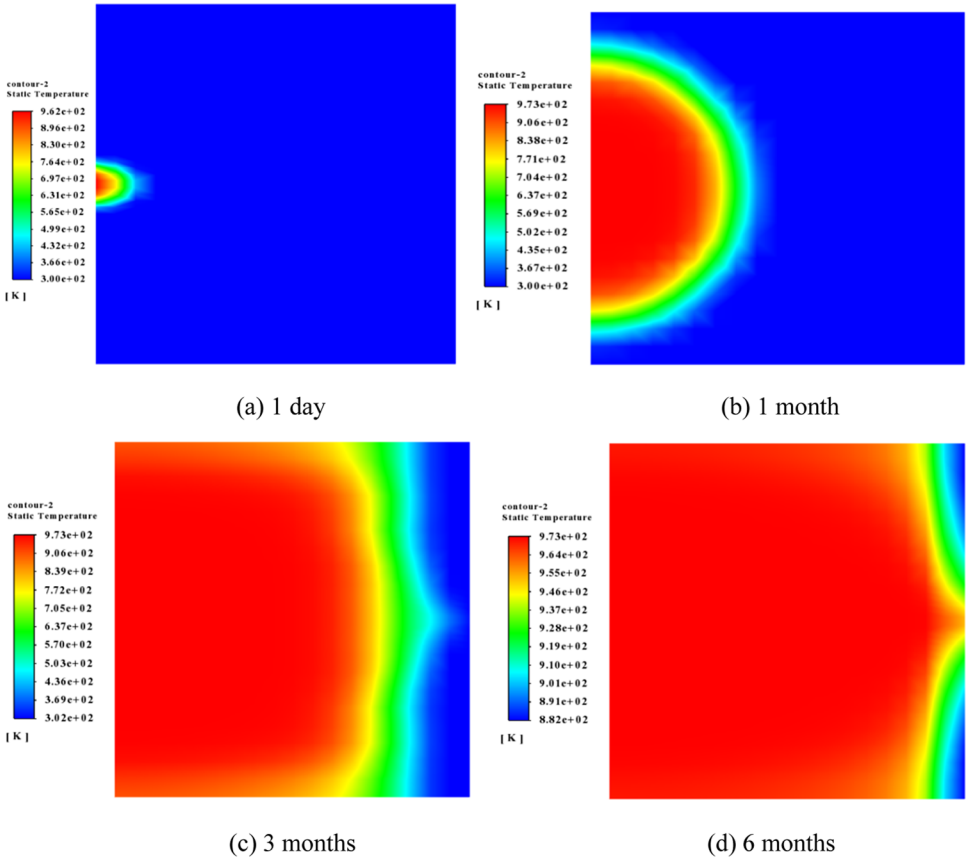

Figure 9. Temperature contours of N_2 injection between the fractured zones (Case 2).

further research on this situation that has not been paid attention to previously.

3.2. Effect of Inlet Velocity. Based on Case 2, the influence of velocity on heat transfer, mass transfer, and oil production is investigated and analyzed in this section.

The development of the temperature field is similar to the results in Figure 9. Moreover, the variation of the temperature field is faster when the inlet velocity is higher. As shown in Figure 14, as the velocity increases, the average temperature curve moves towards the left, reaching a stable temperature faster in the zone. It indicates that increasing the inlet velocity will increase the heating rate and enhance the heat transfer.

As illustrated in Figure 15, the inlet velocity has a positive effect on the increase of the heating rate. As the inlet velocity increases from 0.1 to 0.9 m s^{-1}, the heating rate increases by 7.5 times. The reason lies in the increase of flow velocity and the significant enhancement of convective heat transfer. At the same time, the increase in the heating rate and flow rate leads to a decrease in the main reaction time and heat transfer uniformity by 28%. However, the increase in the velocity leads to differences in the production of different regions, and thus the heat transfer uniformity gets worse.

Figure 16 suggests the variation of the final stable pressure drop under different velocities. It is illustrated that as the velocity increases, the pressure drop increases, which fits the mechanism of Darcy's law. The increase in the pressure drop reveals that there is a linear relationship between flow resistance and velocity in the TCISP process.

It is revealed in Figure 17 that slowing down the flow rate is beneficial to the complete pyrolysis of coal in the region. When the velocity is low enough, more coal is pyrolyzed to produce a little larger amount of oil. With the increase in the flow rate, the conversion rate in the main reaction process increases from 88.15 to 95.67% (the oil content of the tar-rich coal is 10%). However, the decrease in yield is small with the increase in the flow rate. When the velocity is low, the heating time is longer than that at a high velocity, and the cost is larger.

In conclusion, the heating rate increases with increasing velocity, but the temperature uniformity and main reaction time decrease. Meanwhile, the flow resistance gets higher. The decrease in velocity results in an 8.53% increase in yield, but a 185.71% increase in heating time. Therefore, increasing the inlet velocity is beneficial for TCISP.

3.3. Effect of Inlet Temperature. Considering the situation that N_2 injection between the fractured zones, the effect of inlet temperature on heat transfer, mass transfer, and oil production is investigated in this section. As illustrated in Figure 18, when the inlet temperature increases, the heating rate increases first and then decreases. There is an optimal temperature. This is because the temperature has exceeded the maximum temperature of the pyrolysis reaction, and further increasing the temperature has little effect on the reaction. On the contrary, the temperature uniformity is worse due to the higher inlet temperature, thus affecting the heating rate. As the inlet temperature increases, the main reaction time decreases. As the significant reaction stops below 873 K, the main reaction time in the case of 873 K is longer than in other cases. With the increase of the temperature, the heat transfer uniformity gets worse.

It is shown in Figure 19 that as the inlet temperature increases, the stable pressure drop increases first and then

https://doi.org/10.1021/acsomega.3c01481
ACS Omega 2023, 8, 32565−32579

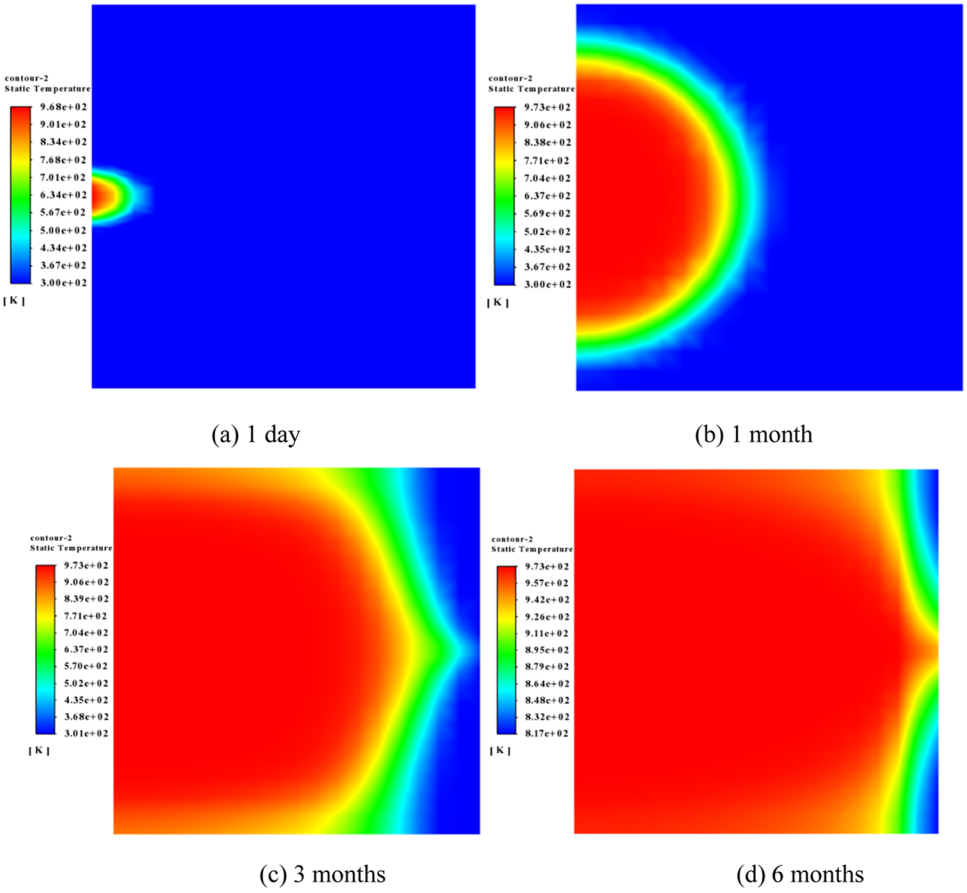

Figure 10. Temperature contours of N_2 injection in the center of the fractured zone (Case 3).

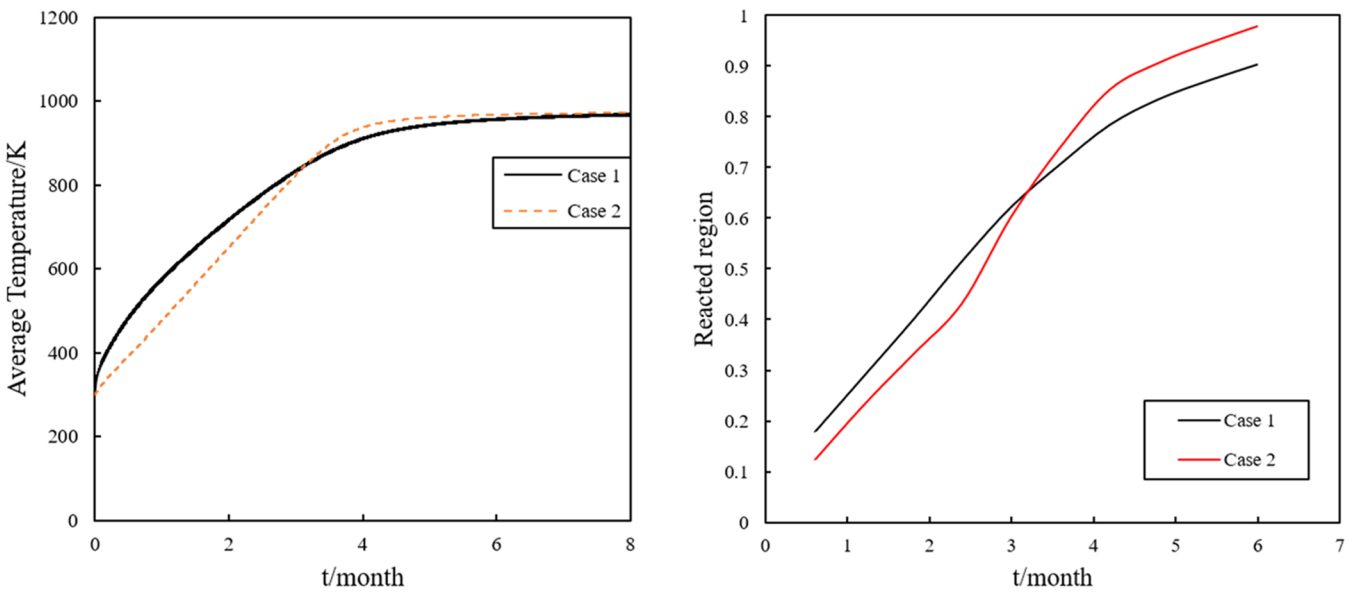

Figure 11. Comparison of the area average temperature and the reacted region for Case 1 and Case 2.

decreases. The stable pressure drop in the case of 973 K is the largest. The pressure drop increases first mainly because of the increase in gas viscosity with increasing temperature. Then, the curve tends to decrease because of less time-average oil production shown in Figure 20.

It is revealed in Figure 20 that with the increase in temperature, the curve tends to be flatter, and the oil-producing time is longer. The mass fraction first increases and then decreases during the process. The gradient of the curve increases and then decreases as the temperature increases when the mass fraction is increasing. This is closely related to the process in which the reaction rate of pyrolysis reaction increases first, then reaches the maximum value, and then

https://doi.org/10.1021/acsomega.3c01481
ACS Omega 2023, 8, 32565−32579

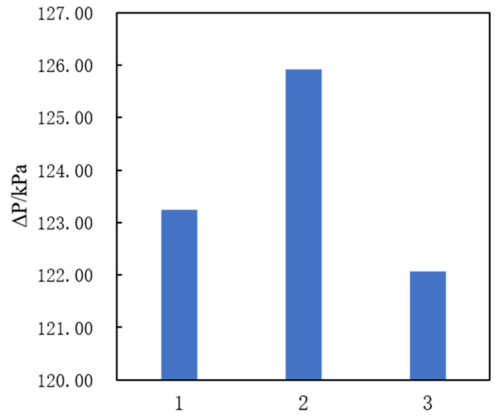

Figure 12. Variation of final stable pressure drop of the three cases.

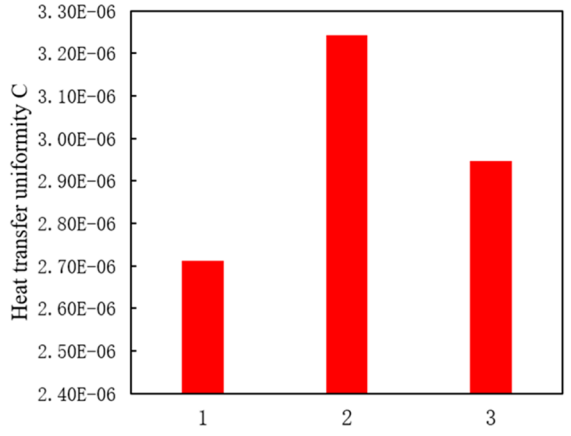

(a) Comparison of the heat transfer uniformity when t is 3 months

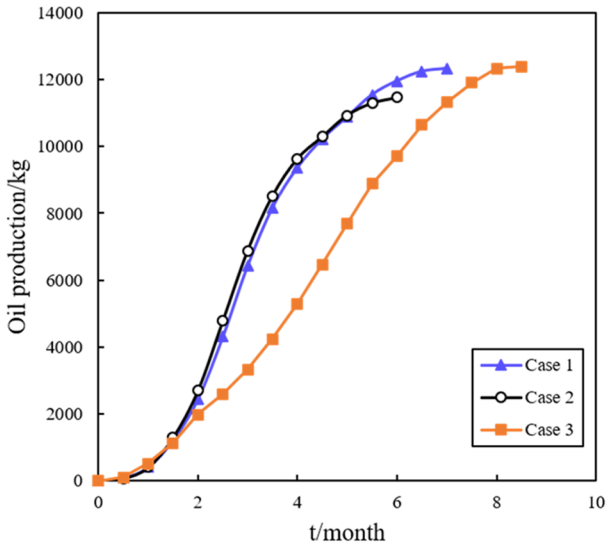

(b) Comparison of the oil production

Figure 13. Comparison of the heat transfer uniformity and the oil production.

decreases. In addition, the maximum value of mass fraction increases with the increase in temperature.

An increase in the inlet temperature is beneficial to the increase in oil production, but the oil production time is increased. There is an optimal inlet temperature for the fastest

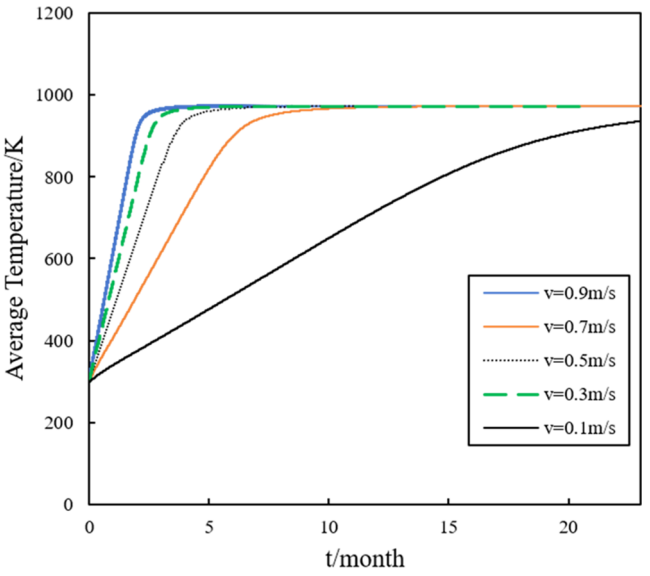

Figure 14. Average temperature curves at different inlet velocities.

heating rate. As the inlet temperature increases, the main reaction time decreases and the heat transfer uniformity gets worse. In conclusion, to maximize the heating rate, the optimum inlet temperature is 973 K.

3.4. Effect of the Fractured Zone Height. The influence of the height of the fractured zone cannot be ignored. The value of height h is 3.6, 4.0, and 4.4 m, respectively, in this section, as shown in Figure 21.

Figure 22 reveals that when the time is 3 months and the corresponding fractured zone height is 3.6, 4.0, and 4.4 m, the maximum heights of the 373 K isotherm in the vertical direction are 8.15, 8.42, and 8.96 m, respectively. Increasing the height of the fractured zone has a positive effect on the vertical expansion of the temperature field.

The results of Figure 23 show that 4.0 m is the best fractured zone height to reduce the flow resistance. Under the condition of constant regional average porosity, with the increase of the height, the low porosity area decreases and the high porosity area increases while the porosity of the high porosity area decreases, so the pressure drop decreases first and then increases.

As shown in Figure 24, it is suggested that as the height increases, the heating rate increases, the main reaction time decreases, and the heat transfer uniformity gets better. As the fractured zone height increases, it is conducive to the gas diffusion to the boundary, so the heating rate increases, the heat transfer uniformity increases, and the residence time decreases. Increasing the height is beneficial for increasing the heating rate and heat transfer uniformity.

It is shown in Figure 25 that the maximum value of the mass fraction of oil increases as the height increases. Moreover, the oil production is 11024.4, 11459.7, and 12001.0 kg, respectively. With the increase in height, the oil production increases from 10824.4 to 12001.0 kg, and the conversion rate increases from 84.8 to 92.3%, indicating the increase of the output to a certain extent. As the height increases, the increase of production decreases because the influence of increasing height on heat and mass transfer decreases.

It is indicated that increasing the height is beneficial for TCISP. Moreover, the yield increases with height under the

https://doi.org/10.1021/acsomega.3c01481
ACS Omega 2023, 8, 32565−32579

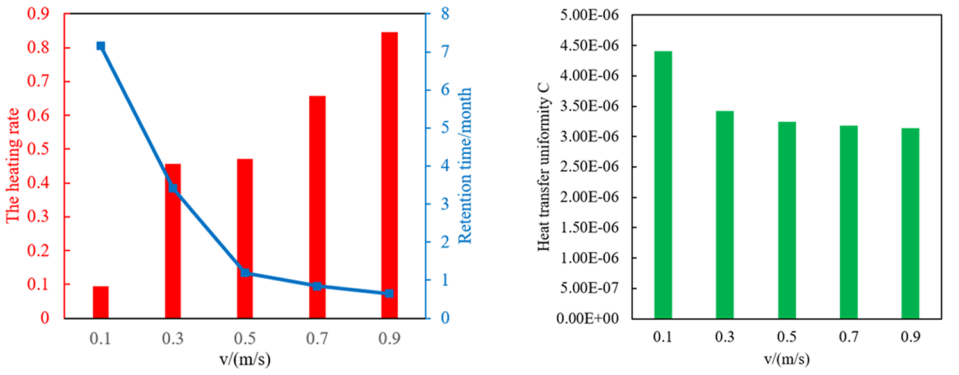

(a) Comparison of Heating rate and main reaction time (b) Comparison of temperature

Figure 15. Comparison of heating rate, main reaction time, and temperature uniformity with velocity.

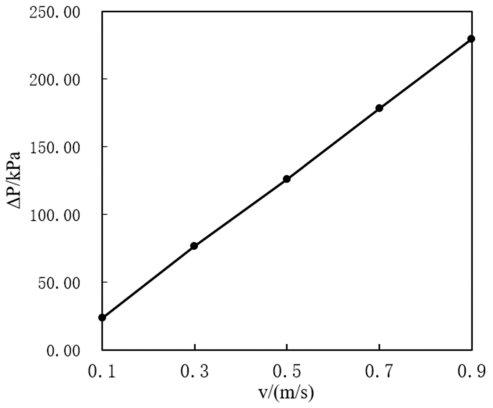

Figure 16. Variation of final stable pressure drop with velocity.

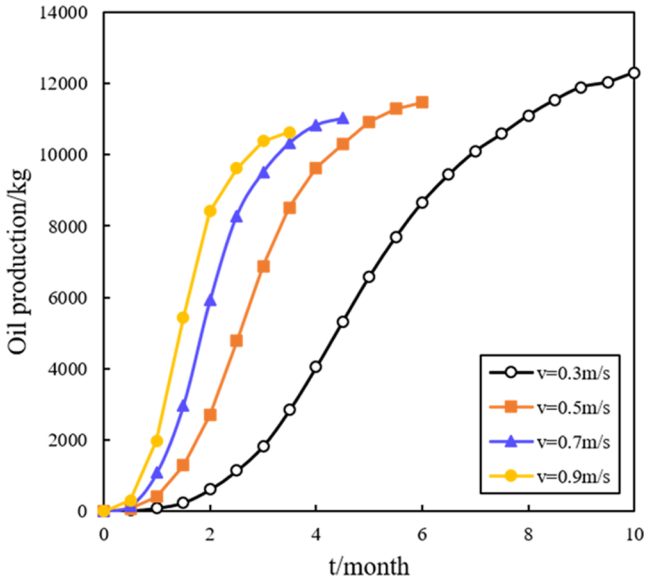

Figure 17. Change of mass fraction of oil at the outlet with time.

conditions investigated. The increment of yield decreases as height increases. Therefore, the enhancement of heat and mass transfer with increasing height has a certain limit.

4. CONCLUSIONS

The macroscopic tar-rich coal in situ pyrolysis (TCISP) multiphysics simulation was carried out numerically, in the practical fractured porous zone, by coupling heat transfer, fluid flow, and chemical reaction. The fractured porous zone was treated as a homogeneous porosity gradient descending region for analysis and practice. A novel TCISP scheme that gas injection between fractured zones was proposed. Moreover, the effect of the fractured porous area, porosity, inlet temperature, inlet velocity, and the height of the fractured porous region on heat transfer, mass transfer, and oil production were investigated. Major conclusions are presented as follows.

(1) Based on the novel simplified method of homogeneous porosity gradient descending treatment of fractured porous zone, a new scheme of large porosity around and small porosity in the center was proposed to realize heat and mass transfer enhancement. The temperature field of N_2 injection between cracks is more uniform, which is conducive to maintaining the same reaction conditions and producing appropriate products. The N_2 injection between cracks is beneficial for TCISP.

(2) Inlet velocity has a significantly positive effect on the increase in heating rate but has a slightly negative effect on heat transfer uniformity. The increase in inlet velocity can slightly increase production. Increasing the inlet velocity could improve the coupling efficiency. Increasing the inlet velocity is beneficial for TCISP.

(3) As the inlet temperature increases from 873 to 1073 K, the heating rate increases first and then decreases. There is an optimal inlet temperature of 973 K for the fastest heating rate. In this case, the heating rate is the fastest and the coupling effect of multiple physical fields is the best.

(4) Increasing the height of the fractured zone is beneficial for increasing the heating rate and heat transfer uniformity. Increasing the height could improve the coupling efficiency. However, the enhancement of heat and mass transfer with increasing height has a certain limit, which is constrained by geometry.

AUTHOR INFORMATION

Corresponding Author

Jinjia Wei − *School of Chemical Engineering and Technology, Xi'an Jiaotong University, Xi'an, Shaanxi 710049, P. R. China;* orcid.org/0000-0001-6373-7374; Email: jjwei@mail.xjtu.edu.cn

https://doi.org/10.1021/acsomega.3c01481
ACS Omega 2023, 8, 32565−32579

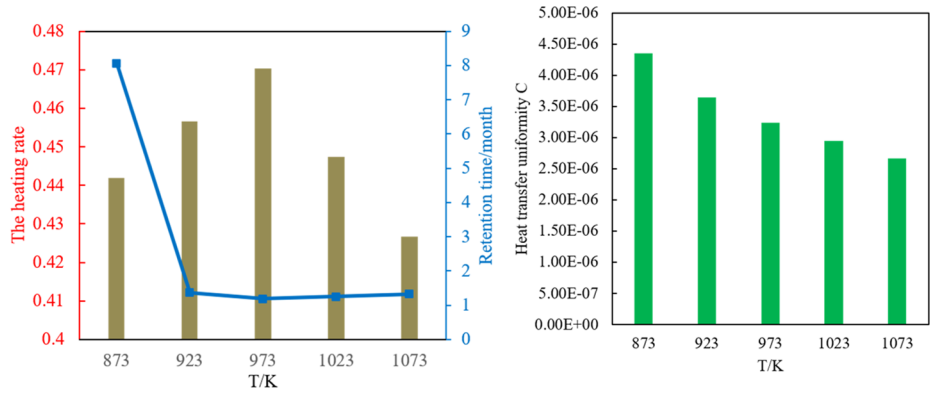

(a) Comparison of Heating rate and main reaction time (b) Comparison of temperature

Figure 18. Comparison of heating rate, main reaction time, and temperature uniformity with inlet temperature.

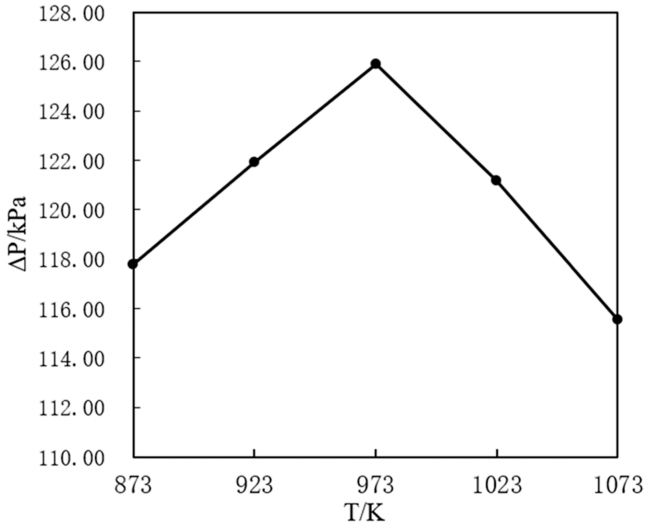

Figure 19. Variation of final stable pressure drop with inlet temperature.

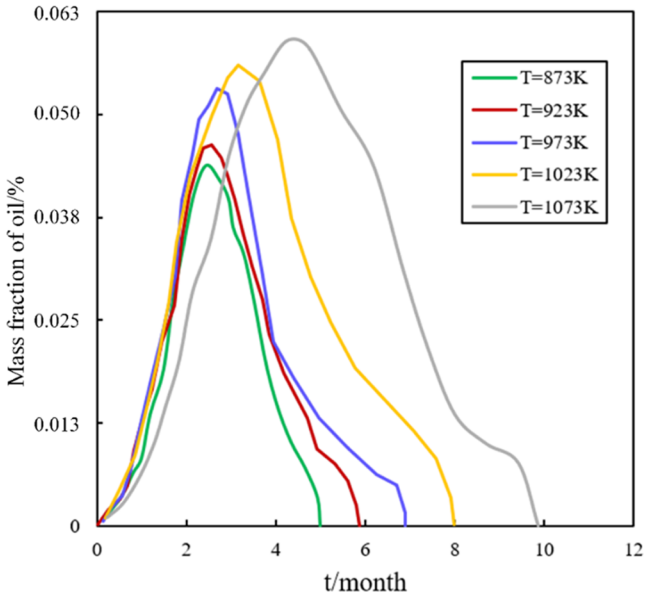

Figure 20. Change of mass fraction of oil at the outlet with time.

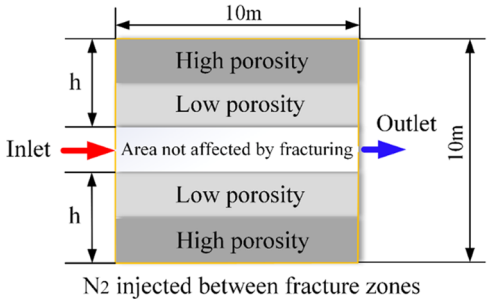

Figure 21. Schematic diagram of the height of the fracture zone.

Authors

Qianhao Ye − *School of Chemical Engineering and Technology, Xi'an Jiaotong University, Xi'an, Shaanxi 710049, P. R. China*

Mingjie Li − *School of Chemical Engineering and Technology, Xi'an Jiaotong University, Xi'an, Shaanxi 710049, P. R. China;* orcid.org/0000-0002-9954-4870

Jingyuan Hao − *School of Chemical Engineering and Technology, Xi'an Jiaotong University, Xi'an, Shaanxi 710049, P. R. China*

Zibo Huang − *School of Chemical Engineering and Technology, Xi'an Jiaotong University, Xi'an, Shaanxi 710049, P. R. China*

Complete contact information is available at: https://pubs.acs.org/10.1021/acsomega.3c01481

Notes

The authors declare no competing financial interest.

■ ACKNOWLEDGMENTS

This work was supported by the Special Project of Science and Technology Energy Security Technology from China Huaneng Group (No. HNKJ20-H87-03) and the research Project of Shaanxi Provincial Coal Geology Group (No. SMDZ-2020ZD-1-03).

■ NOMENCLATURE

ε:porosity
t:time [s]
$\vec{v}$:velocity vector [m s^{-1}]
P:pressure [Pa]
K:permeability [m^2]

https://doi.org/10.1021/acsomega.3c01481
ACS Omega 2023, 8, 32565−32579

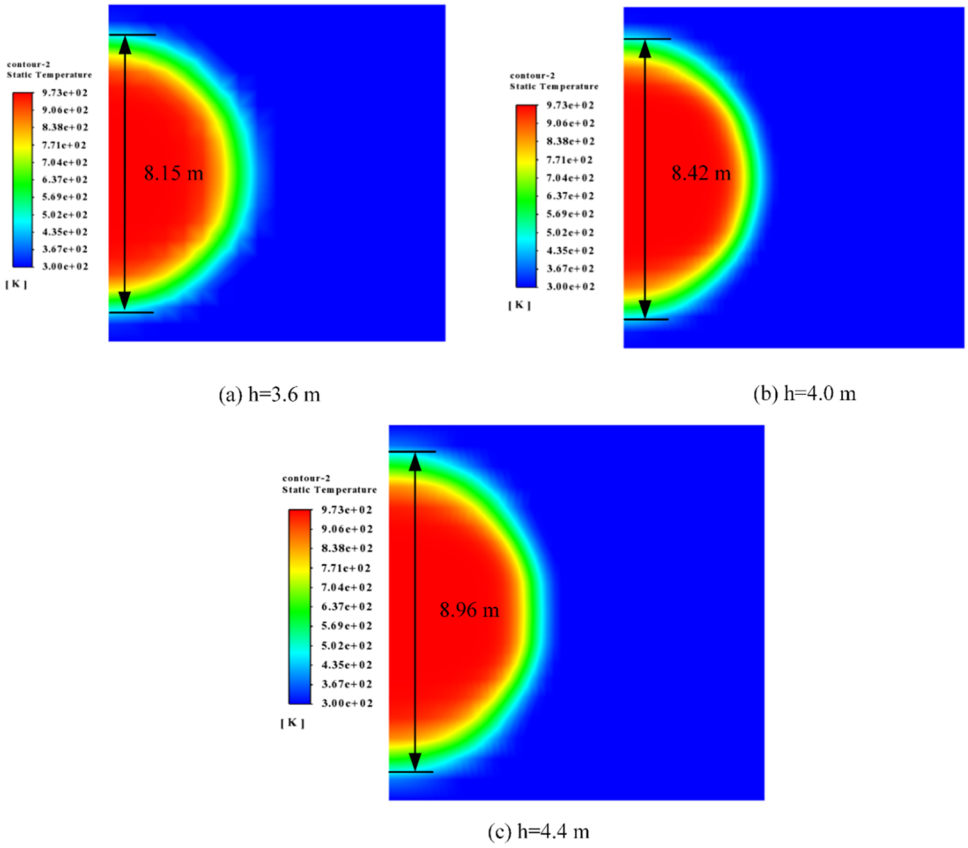

(a) h=3.6 m (b) h=4.0 m

(c) h=4.4 m

Figure 22. Temperature contours of different heights of the fractured zone when t = 3 months.

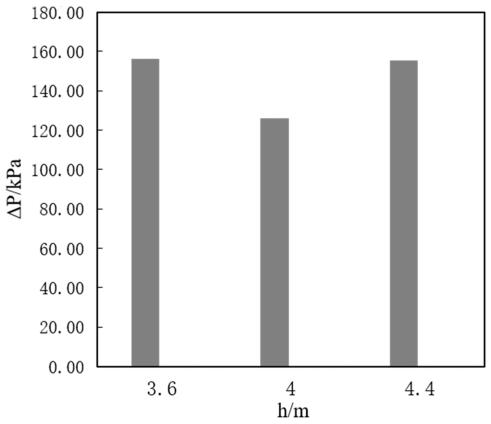

Figure 23. Variation of final stable pressure drop with different heights of the fractured zone.

T:temperature [K]
μ:dynamic viscosity [Pa·s]
λ:thermal conductivity [W·m^{-1} K^{-1}]
ρ:density [kg·m^{-3}]
A:pre-exponential [s^{-1}]
m:temperature index
E_0:activation energy [J·mol^{-1}]
R:mole gas constant [J·mol^{-1} K^{-1}]
q_R:mass rate of reaction [kg·m^{-3} s^{-1}]
c_p:heat capacity [J·kg^{-1} K^{-1}]
X_i:mass fraction of the ith component
c_p:heat capacity [J·kg^{-1} K^{-1}]
ΔH:enthalpy of reaction [J·mol^{-1} kg^{-1}]
k:reaction rate [mol·m^{-3} s^{-1}]
k_f:correction coefficient of the reaction rate

SUBSCRIPTS

i:index of variables
N:final index of variables
s:solid
g:gas

ACRONYMS

TCISP:tar-rich coal in situ pyrolysis
UCG:underground coal gasification
ISU:in situ upgrading

REFERENCES

(1) Fan, Y.; Durlofsky, L.; Tchelepi, H. Numerical simulation of the in-situ upgrading of oil shale. *SPE J.* **2010**, *15*, 368−381.
(2) Maes, J.; Muggeridge, A. H.; Jackson, M. D.; et al. Scaling analysis of the In-Situ Upgrading of heavy oil and oil shale. *Fuel* **2017**, *195*, 299−313.
(3) Bauman, J. H.; Huang, C. K.; Gani, M. R.; et al. Modeling of the in-situ production of oil from oil shale. *ACS Symp. Ser.* **2010**, *1032*, 135−146.
(4) Hao, Y.; Yunxing, D. A feasibility study on in-situ heating of oil shale with injection fluid in China. *J. Pet. Sci. Eng.* **2014**, *122*, 304−317.
(5) Lei, G.; et al. Numerical simulation on in-situ upgrading of oil shale via steam injection. *J. China Univ. Pet.* **2017**, *41*, 100−107.
(6) Pei, S.; Wang, Y.; Zhang, L.; et al. An innovative nitrogen injection assisted in-situ conversion process for oil shale recovery: mechanism and reservoir simulation study. *J. Pet. Sci. Eng.* **2018**, *171*, 507−515.

https://doi.org/10.1021/acsomega.3c01481
ACS Omega 2023, 8, 32565−32579

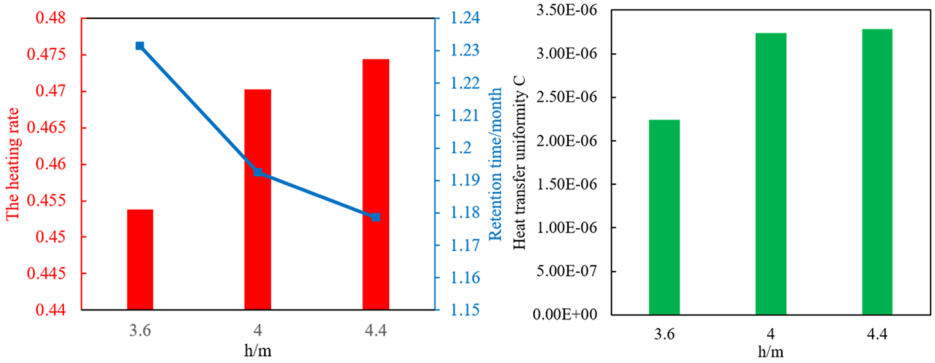

(a) Comparison of Heating rate and main reaction time (b) Comparison of temperature

Figure 24. Comparison of heating rate, main reaction time, and temperature uniformity with different heights of the fractured zone.

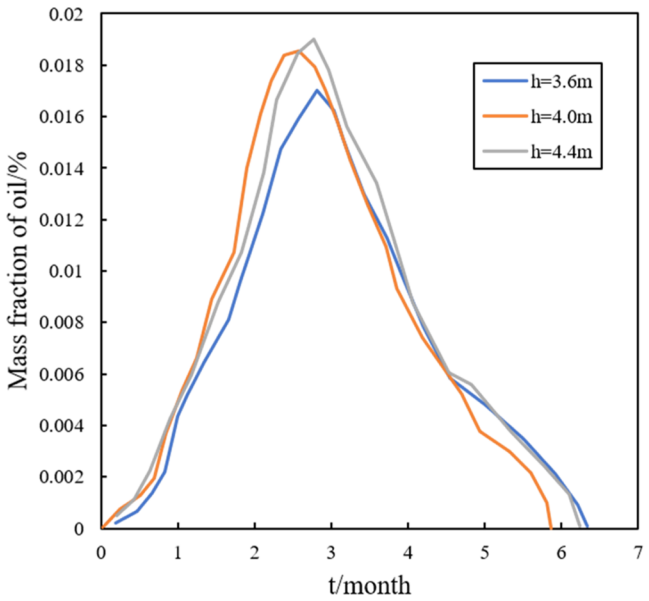

Figure 25. Change of mass fraction of oil at the outlet with time.

(7) Pei, S.; Cui, G. D.; et al. Air assisted in situ upgrading via underground heating for ultra heavy oil: experimental and numerical simulation study. *Fuel* **2020**, *279*, No. 118452.
(8) Pei, S.; Huang, L. J.; et al. Experimental study on thermal cracking reactions of ultra-heavy oils during air injection assisted in-situ upgrading process. *J. Pet. Sci. Eng.* **2020**, *195*, No. 107850.
(9) Pei, S.; Cui, G.; et al. Performance and important engineering aspects of air injection assisted in situ upgrading process for heavy oil recovery. *J. Pet. Sci. Eng.* **2021**, *202*, No. 108554.
(10) Varfolomeev, M. A.; Galukhin, A.; et al. Thermal decomposition of Tatarstan Ashal'cha heavy crude oil and its SARA fractions. *Fuel* **2016**, *186*, 122−127.
(11) Varfolomeev, M. A.; Nagrimanov, R. N.; Galukhin, A. V.; et al. Contribution of thermal analysis and kinetics of Siberian and Tatarstan regions crude oils for in situ combustion process. *J. Therm. Anal. Calorim.* **2015**, *122*, 1375−1384.
(12) Varfolomeev, M. A.; Nurgaliev, D.; Kok, M. V. Thermal, kinetics, and oxidation mechanism studies of light crude oils in limestone and sandstone matrix using TG-DTG-DTA: effect of heating rate and mesh size. *Pet. Sci. Technol.* **2016**, *34*, 1647−1653.
(13) Chen, Y.-f.; Pu, W. f.; Liu, X. l.; et al. A preliminary feasibility analysis of in situ combustion in a deep fractured-cave carbonate heavy oil reservoir. *J. Pet. Sci. Eng.* **2019**, *174*, 446−455.
(14) Chen, Y.; Pu, W.; Liu, X.; et al. Specific kinetic triplet estimation of Tahe heavy oil oxidation reaction based on non-isothermal kinetic results. *Fuel* **2019**, *242*, 545−552.
(15) Yang, L.; Yang, D.; et al. Changes of oil shale pore structure and permeability at different temperatures. *Oil Shale* **2016**, *33*, 101−110.
(16) Han, X.; Jiang, X.; et al. Effects of Retorting Factors on Combustion Properties of Shale Char. 2. Pore Structure. *Energy Fuels* **2011**, *25*, 97−102.
(17) Sun, L.; Tuo, J.; et al. Formation and development of the pore structure in Chang 7 member oil-shale from Ordos Basin during organic matter evolution induced by hydrous pyrolysis. *Fuel* **2015**, *158*, 549−557.
(18) Qing, W.; Jiao, G.; et al. Variation of the pore structure during microwave pyrolysis of oil shale. *Oil Shale* **2010**, *27*, 135−146.
(19) Geng, Y.; Liang, W.; et al. Evolution of Pore and Fracture Structure of Oil Shale under high temperature and high pressure. *Energy Fuels* **2017**, *31*, 10404−10413.
(20) Yang, L.; Liu, S. Numerical simulation on heat and mass transfer in the process of underground coal gasification. *Numer. Heat Transfer, Part A* **2003**, *44*, 537−557.
(21) Yang, L. Study on the model experiment and numerical simulation for underground coal gasification. *Fuel* **2004**, *83*, 573−584.
(22) Yang, L. Nonlinear coupling mathematical models on percolation-patterned underground coal gasification. *Int. J. Energy Res.* **2005**, *29*, 1331−1353.
(23) Seifi, M.; Chen, Z.; Abedi, J. Numerical simulation of underground coal gasification using the CRIP method. *Can. J. Chem. Eng.* **2011**, *89*, 1528−1535.
(24) Seifi, M.; Abedi, J.; Chen, Z. Application of porous medium approach to simulate UCG process. *Fuel* **2014**, *116*, 191−200.
(25) Nourozieh, H.; Kariznovi, M.; et al. Simulation study of underground coal gasification in Alberta reservoirs: geological structure and process modeling. *Energy Fuels* **2010**, *24*, 3540−3550.
(26) żogała, A.; Janoszek, T. CFD simulations of influence of steam in gasification agent on parameters of UCG process. *J. Sustainable Min.* **2015**, *14*, 2−11.
(27) Wachowicz, J.; Łączny, J.; et al. Modelling of underground coal gasification process using CFD methods. *Arch. Min. Sci.* **2015**, *60*, 663−676.
(28) Gür, M.; Canbaz, E. Analysis of syngas production and reaction zones in hydrogen oriented underground coal gasification. *Fuel* **2020**, *269*, No. 117331.
(29) Nurzynska, K.; Janoszek, T.; Iwaszenko, S. In *Modelling Test of Cavity Growth During Underground Coal Gasification Process Using CFD Method*, 2014 International Conference on Information Science, Electronics and Electrical Engineering, IEEE, 2014; pp 415−419.
(30) Jiang, L.; Chen, Z.; Farouq Ali, S. Thermal-hydro-chemical-mechanical alteration of coal pores in underground coal gasification. *Fuel* **2020**, *262*, No. 116543.
(31) Gao, W.; Zagorščak, R.; Thomas, H. R. Insights into solid-gas conversion and cavity growth during Underground Coal Gasification

https://doi.org/10.1021/acsomega.3c01481
ACS Omega 2023, 8, 32565−32579

(UCG) through Thermo-Hydraulic-Chemical (THC) modelling. *Int. J. Coal Geol.* **2021**, *237*, No. 103711.
(32) Schaube, F.; Kohzer, A.; et al. De- and rehydration of Ca(OH)2 in a reactor with direct heat transfer for thermo-chemical heat storage. Part A: Experimental results. *Chem. Eng. Res. Des.* **2013**, *91*, 856−864.
(33) Schaube, F.; Utz, I.; et al. De- and rehydration of Ca (OH)2 in a reactor with direct heat transfer for thermo-chemical heat storage. Part B: Validation of model. *Chem. Eng. Res. Des.* **2013**, *91*, 865−873.
(34) Shi, T.; Xu, H.; et al. Multi-physics modeling of thermochemical heat storage with enhance heat transfer. *Appl. Therm. Eng.* **2021**, *198*, No. 117508.
(35) Zhang, T.; Li, Y.; Cai, J. et al. *A Digital Twin for Unconventional Reservoirs: A Multiscale Modeling and Algorithm to Investigate Complex Mechanisms*; Geofluids, 2020.
(36) Zhang, T.; Zhang, Y.; Katterbauer, K.; et al. Phase equilibrium in the hydrogen energy chain. *Fuel* **2022**, *328*, No. 125324.

https://doi.org/10.1021/acsomega.3c01481
ACS Omega 2023, 8, 32565−32579